An assessment of a co-rotational EAS brick element

Abstract

A locking-free formulation of 8-node brick element and its application is demonstrated. The Enhanced Assumed Strain (EAS) method is used to alleviate the locking problems. A co-rotational formulation is adopted in the formulation, thus geometric nonlinearity is taken into account via rotation of the local coordinate system. Several benchmark problems are analyzed to demonstrate the efficiency of the element.

Keywords

brick element, co-rotational formulation, EAS method.

Cengiz Polat[*]

Firat University, Faculty of Engineering, Department of Civil Engineering, 23279, Elazig – Turkey
Fax: +90 424 218 89 42

[*] Author email: cpolat@firat.edu.tr

1 INTRODUCTION

In the linear analysis, the displacements and strains developed in the structure are small. That is, the geometry of the structure assumed remains unchanged during the loading process and linear strain approximations can be used. However, the geometry of the structure changes continuously during the loading process, and this fact is taken into account in the geometrically nonlinear analysis. Three Lagrangian kinematical descriptions are in present use for finite element analysis of geometrically nonlinear structures: Total Lagrangian (TL), Updated Lagrangian (UL) and Co-rotational (CR) formulation [5]. The pioneers of the co-rotational approach can be said as Wempner [15], Argyris et al. [2], Belytschko and Glaum [3], Crisfield and Moita [4] and Moita and Crisfield [9]. The attractiveness of the CR formulation resides in the fact that it can be applied to simplify the Lagrangian formulations for large-displacement and small-strain problems without significant loss of accuracy [13]. In this formulation the rigid-body motion is eliminated and only element deformation is considered to obtain the internal forces and the tangent stiffness matrix.

The objective of this paper is to demonstrate the locking-free formulation of 8-node brick element based on the co-rotational description of motion. Firstly, the geometry and the strain-displacement relations of the displacement based 8-node brick element are presented. To alleviate the locking phenomenon of the element, the Enhanced Assumed Strain (EAS) method that was presented for the first time by Simo and Rifai [11] and further developed by Andelfinger and Ramm [1], is used. The EAS method is based on the enhancing of the displacement-dependent strain field by an extra assumed strain field, and it is assumed that the stress and

the enhanced assumed strain fields are orthogonal, which results in an elimination of the stress field from the finite element equations. Secondly, a co-rotational formulation [4, 5, 9] is given. A local coordinate system is attached to the element and a rotation matrix which defines the rotation of this local coordinate system according to the global coordinate system, is obtained using the polar decomposition theorem. Thus, the geometric non-linearity is incorporated by the rotation of the local coordinate system. Lastly, several benchmark problems are examined by a computer program which is written by the author in MATLAB code.

2   ELEMENT FORMULATION

2.1   Geometry of the brick element

The coordinates of a typical point in the brick element (Fig. 1) can be written as

$$\mathbf{x} = \sum_{k=1}^{n} N_k x_k \tag{1}$$

where n is the number of nodes, $N_k = N_k(\xi, \eta, \zeta)$ are the three-dimensional isoparametric shape functions, $\mathbf{x} = \begin{bmatrix} x & y & z \end{bmatrix}^T$ are the position vectors; ξ, η and ζ are the curvilinear coordinates. Here ξ, η and ζ are assumed to vary from -1 and +1.

The displacement field $\mathbf{u} = \begin{bmatrix} u & v & w \end{bmatrix}^T$ in the brick element can be approximated by

$$\mathbf{u} = \sum_{k=1}^{n} N_k u_k \tag{2}$$

where $\mathbf{u}_k = \begin{bmatrix} u_k & v_k & w_k \end{bmatrix}^T$ represents the displacement vector of node k.
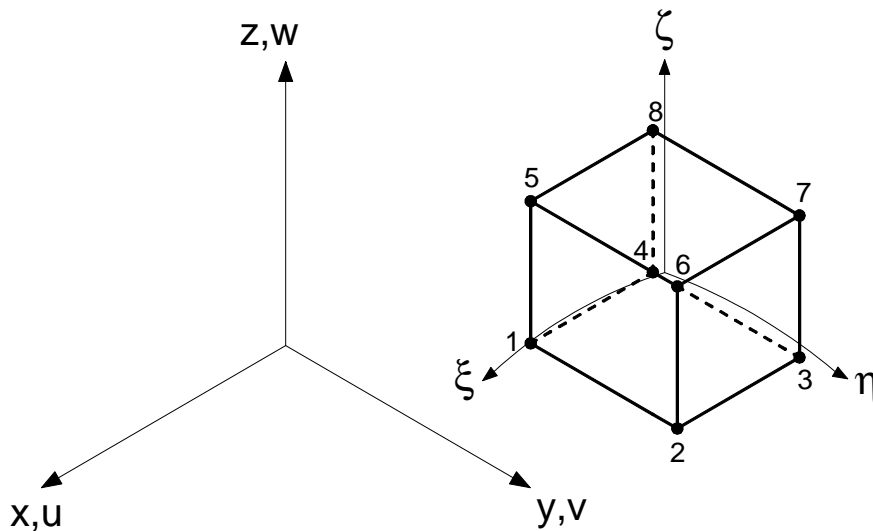
Figure 1   Geometrical description of the eight-node brick element.

2.2   Strain-displacement relationships

The components of the strain tensor $\boldsymbol{\varepsilon}^u$ in the natural set of coordinates (ξ, η, ζ) can be given as

$$\boldsymbol{\varepsilon}^u = \left[\begin{array}{cccccc} \varepsilon_{\xi\xi}^u & \varepsilon_{\eta\eta}^u & \varepsilon_{\zeta\zeta}^u & \varepsilon_{\xi\eta}^u & \varepsilon_{\xi\zeta}^u & \varepsilon_{\eta\zeta}^u \end{array} \right]^T \tag{3}$$

or

$$\boldsymbol{\varepsilon}^u = \mathbf{B}^u \mathbf{u} \; ; \quad \mathbf{u} = \left[\begin{array}{ccc} \mathbf{u}_1 & \dots & \mathbf{u}_k \end{array} \right]^T \quad k = 1, \dots n \tag{4}$$

where $\mathbf{B}^u$ is the conventional strain-displacement matrix and $\mathbf{u}$ is the nodal displacement vector.

The natural strain components defined in Equation (3) can be determined [12] by using the displacement vector $\mathbf{u}$ and the covariant base vectors $\mathbf{g}_i$ as

$$\varepsilon_{\xi_i \xi_j}^u = \frac{1}{2} \left(\frac{\partial \mathbf{u}}{\partial \xi_i} \mathbf{g}_j + \frac{\partial \mathbf{u}}{\partial \xi_j} \mathbf{g}_i \right) \quad i, j = 1, 2, 3; \; \xi_1 = \xi; \; \xi_2 = \eta; \; \xi_3 = \zeta \tag{5}$$

$$\mathbf{g}_i = \frac{\partial \mathbf{x}}{\partial \xi_i} \tag{6}$$

where $\mathbf{x}$ is the position vector.

In the pure displacement-based finite element formulation, employing the full quadrature rules leads to some locking effects. To resolve these locking problems without reducing the quadrature rules, the displacement-based strain field can be enhanced as follows;

$$\boldsymbol{\varepsilon} = \boldsymbol{\varepsilon}^u + \boldsymbol{\varepsilon}^\alpha \tag{7}$$

where $\boldsymbol{\varepsilon}$ is the improved strain field and $\boldsymbol{\varepsilon}^\alpha$ is the additive enhanced strain field. The additive enhanced strain field can be rewritten as

$$\boldsymbol{\varepsilon}^\alpha = \mathbf{B}^\alpha \boldsymbol{\alpha} \; ; ; \quad \boldsymbol{\alpha} = \left[\begin{array}{ccc} \alpha_1 & \dots & \alpha_k \end{array} \right]^T \quad k = 1, \dots 30 \tag{8}$$

where $\mathbf{B}^\alpha$ and is the EAS-based strain-displacement matrix, α is vector of EAS variables. This matrix is given by [10].

$$\mathbf{B}^\alpha = \left[\begin{array}{ccc|cccccc|cccccc|cccccc|ccc|cccccc} \xi & 0 & 0 & 0 & 0 & 0 & 0 & 0 & 0 & 0 & 0 & 0 & 0 & 0 & 0 & \xi\eta & \xi\zeta & 0 & 0 & 0 & 0 & 0 & 0 & 0 & \xi\eta\zeta & 0 & 0 & 0 & 0 & 0 \\ 0 & \eta & 0 & 0 & 0 & 0 & 0 & 0 & 0 & 0 & 0 & 0 & 0 & 0 & 0 & 0 & 0 & \xi\eta & \eta\zeta & 0 & 0 & 0 & 0 & 0 & 0 & \xi\eta\zeta & 0 & 0 & 0 & 0 \\ 0 & 0 & \zeta & 0 & 0 & 0 & 0 & 0 & 0 & 0 & 0 & 0 & 0 & 0 & 0 & 0 & 0 & 0 & 0 & \xi\zeta & \eta\zeta & 0 & 0 & 0 & 0 & 0 & \xi\eta\zeta & 0 & 0 & 0 \\ 0 & 0 & 0 & \xi & \eta & 0 & 0 & 0 & 0 & \xi\zeta & \eta\zeta & 0 & 0 & 0 & 0 & 0 & 0 & 0 & 0 & 0 & 0 & \xi\eta & 0 & 0 & 0 & 0 & 0 & \xi\eta\zeta & 0 & 0 \\ 0 & 0 & 0 & 0 & 0 & \xi & \zeta & 0 & 0 & 0 & 0 & \xi\eta & \eta\zeta & 0 & 0 & 0 & 0 & 0 & 0 & 0 & 0 & 0 & \xi\zeta & 0 & 0 & 0 & 0 & 0 & \xi\eta\zeta & 0 \\ 0 & 0 & 0 & 0 & 0 & 0 & \eta & \zeta & 0 & 0 & 0 & 0 & 0 & \xi\eta & \xi\zeta & 0 & 0 & 0 & 0 & 0 & 0 & 0 & 0 & \eta\zeta & 0 & 0 & 0 & 0 & 0 & \xi\eta\zeta \end{array} \right] \tag{9}$$

The previously described strain field was related to the natural set of coordinates. Therefore, these strains can be transformed onto the local coordinate system by a transformation matrix $\mathbf{T}_0$ such as

$$\mathbf{T}_0 = \begin{bmatrix} J_0 J_0 & J_0 J_0 & J_0 J_0 & J_0 J_0 & J_0 J_0 & J_0 J_0 \\ J_0 J_0 & J_0 J_0 & J_0 J_0 & J_0 J_0 & J_0 J_0 & J_0 J_0 \\ J_0 J_0 & J_0 J_0 & J_0 J_0 & J_0 J_0 & J_0 J_0 & J_0 J_0 \\ 2J_0 J_0 & 2J_0 J_0 & 2J_0 J_0 & J_0 J_0 + J_0 J_0 & J_0 J_0 + J_0 J_0 & J_0 J_0 + J_0 J_0 \\ 2J_0 J_0 & 2J_0 J_0 & 2J_0 J_0 & J_0 J_0 + J_0 J_0 & J_0 J_0 + J_0 J_0 & J_0 J_0 + J_0 J_0 \\ 2J_0 J_0 & 2J_0 J_0 & 2J_0 J_0 & J_0 J_0 + J_0 J_0 & J_0 J_0 + J_0 J_0 & J_0 J_0 + J_0 J_0 \end{bmatrix}^{-1} \tag{10}$$

in which $\mathbf{J}_0$ is the conventional Jacobian matrix which is evaluated at the element center

$$\mathbf{J}_0 = \begin{bmatrix} \frac{\partial x}{\partial \xi} & \frac{\partial y}{\partial \xi} & \frac{\partial z}{\partial \xi} \\ \frac{\partial x}{\partial \eta} & \frac{\partial y}{\partial \eta} & \frac{\partial z}{\partial \eta} \\ \frac{\partial x}{\partial \zeta} & \frac{\partial y}{\partial \zeta} & \frac{\partial z}{\partial \zeta} \end{bmatrix} \tag{11}$$

The natural coordinate and the local coordinate system can be related by the second-order transformation tensor. Thus, the strain components in the local frame $\bar{\varepsilon}$

$$\bar{\varepsilon}^u = \begin{bmatrix} \bar{\varepsilon}^u_{xx} & \bar{\varepsilon}^u_{yy} & \bar{\varepsilon}^u_{zz} & \bar{\varepsilon}^u_{xy} & \bar{\varepsilon}^u_{xz} & \bar{\varepsilon}^u_{yz} \end{bmatrix}^T \tag{12}$$

$$\bar{\varepsilon}^u = \mathbf{T}_0 \varepsilon^u = \overline{\mathbf{B}}^u \mathbf{u} \tag{13}$$

$$\bar{\varepsilon}^\alpha = \frac{det\mathbf{J}_0}{det\mathbf{J}} \mathbf{T}_0 \varepsilon^\alpha = \overline{\mathbf{B}}^\alpha \boldsymbol{\alpha} \tag{14}$$

where $\mathbf{J}$ is the Jacobian matrix.

2.3   Co-rotational formulation

The initial local system coordinates $\mathbf{X}_l^k$ of node k can be given as

$$\mathbf{X}_l^k = \mathbf{X}^k - \mathbf{X}^1 \tag{15}$$

It is considered that the initial coordinates in the local and global systems are the same. In order to obtain the local axes within the nonlinear process, it is necessary to determine the rotation matrix $\mathbf{R}$. The incremental global deformation gradient $\mathbf{F}$ computed at the center of the element can be written as

$$\mathbf{F} = \mathbf{R}\mathbf{U} \tag{16}$$

where $\mathbf{U}$ is right stretch tensor. The rotation matrix can be evaluated from the well known polar decomposition theorem, mostly with the determination of the eigenvalues of the right Cauchy-Green tensor [14].

Thus, the rotation matrix $\mathbf{R}$ is

$$\mathbf{R} = \begin{bmatrix} \mathbf{e_1} & \mathbf{e_2} & \mathbf{e_3} \end{bmatrix} \tag{17}$$

where $\mathbf{e_1}$, $\mathbf{e_2}$ and $\mathbf{e_3}$ are the local rotated unit vectors. The relationship between the local and global current position vectors of node k is explicitly given by

$$\mathbf{x}_l^k = \mathbf{X}_l^k + \mathbf{u}_l^k = \begin{pmatrix} X_l \\ Y_l \\ Z_l \end{pmatrix}^k + \begin{pmatrix} u_l \\ v_l \\ w_l \end{pmatrix}^k = \mathbf{R}^T \left(\mathbf{x}_g^k - \mathbf{x}_g^1 \right) = \mathbf{R}^T \mathbf{x}_g^{k_1} \tag{18}$$

where $\mathbf{x}_l^k$ and $\mathbf{x}_g^k$ are the current coordinates for the local and global position vectors for the node k, respectively.

The variation of Eq. (18) gives the relationship between the variation of the local displacements and the variation of the global displacements,

$$\delta \mathbf{u}_l^k = \mathbf{R}^T \delta \mathbf{u}_g^k + \delta \mathbf{R}^T \mathbf{x}_g^{k1} \tag{19}$$

We can rewrite Eq. (19) using a skew-symmetric matrix $\mathbf{S}$

$$\delta \mathbf{u}_l^k = \mathbf{R}^T \delta \mathbf{u}_g^k + \mathbf{R}^T \mathbf{S} \left(\mathbf{x}_g^{k_1} \right) \delta \boldsymbol{\theta} \tag{20}$$

$$\mathbf{S} \left(\mathbf{x}_g^{k_1} \right) = \begin{bmatrix} 0 & -z_g^{k_1} & y_g^{k_1} \\ z_g^{k_1} & 0 & -x_g^{k_1} \\ -y_g^{k_1} & x_g^{k_1} & 0 \end{bmatrix} \tag{21}$$

we can rewrite Eq. (20) at the element level as

$$\delta \mathbf{u}_l = \left[\operatorname{diag} \mathbf{R}^T \right] \delta \mathbf{u}_g + \operatorname{col} \left(\mathbf{R}^T \mathbf{S} \left(\mathbf{x}_g^{k_1} \right) \right) \delta \boldsymbol{\theta} \tag{22}$$

where $\delta \boldsymbol{\theta}$ is a pseudo-vector. To find an expression for the pseudo-vector $\delta \boldsymbol{\theta}$, we can write a spin vector $\boldsymbol{\Omega}$ using local quantities

$$\boldsymbol{\Omega} = \begin{bmatrix} \frac{\partial u_l}{\partial Y_l} - \frac{\partial v_l}{\partial X_l} \\ \frac{\partial u_l}{\partial Z_l} - \frac{\partial w_l}{\partial X_l} \\ \frac{\partial v_l}{\partial Z_l} - \frac{\partial w_l}{\partial Y_l} \end{bmatrix} = \mathbf{A}_l^T \mathbf{u}_l = 0 \tag{23}$$

where $\mathbf{A}_l$ is the 24x3 matrix. Differentiating of this spin vector we can get

$$\delta \boldsymbol{\Omega} = \mathbf{A}_l^T \delta \mathbf{u}_l = \mathbf{A}_l^T \left[\operatorname{diag} \mathbf{R}^T \right] \delta \mathbf{u}_g + \mathbf{A}_l^T \operatorname{col} \left(\mathbf{R}^T \mathbf{S} \left(x_g^{k_1} \right) \right) \delta \boldsymbol{\theta} = 0 \tag{24}$$

and

$$\delta \boldsymbol{\theta} = - \left[\mathbf{A}_l^T \operatorname{col} \left(\mathbf{R}^T \mathbf{S} \left(\mathbf{x}_g^{k_1} \right) \right) \right]^{-1} \mathbf{A}_l^T \left[\operatorname{diag} \mathbf{R}^T \right] \delta \mathbf{u}_g = \mathbf{V}^T \delta \mathbf{u}_g \tag{25}$$

Consequently using Eq. (22) an Eq. (25)

$$\delta u_l = \left[\left[\operatorname{diag} \mathbf{R}^T \right] + \operatorname{col} \left(\mathbf{R}^T \mathbf{S} \left(\mathbf{x}_g^{k1} \right) \right) \mathbf{V}^T \right] \delta \mathbf{u}_g = \mathbf{T} \delta \mathbf{u}_g \tag{26}$$

where $\mathbf{T}$ is transformation matrix.

2.4   Tangent stiffness matrix

The local internal force vector $\mathbf{F}_{i,l}$ for the 8-node brick element can be determined via

$$\mathbf{F}_{i,l} = \int \overline{\mathbf{B}}_l^u \boldsymbol{\sigma}_l dV_0 \tag{27}$$

where $\mathbf{B}_l$ is the strain-displacement matrix, $\boldsymbol{\sigma}_l$ is the local stresses. The relationship between the global and local internal force vectors can be given as

$$\mathbf{F}_{i,g} = \mathbf{T}^T \mathbf{F}_{i,l} = \mathbf{T}^T \mathbf{K}_l \mathbf{u}_l \tag{28}$$

where $\mathbf{K}_l$ is the linear local stiffness matrix. The global tangent stiffness matrix $\mathbf{K}_T$ can be determined via differentiation of Eq. (28) such as

$$\delta\mathbf{F}_{i,g} = \mathbf{T}^T \delta\mathbf{F}_{i,l} + \delta\mathbf{T}^T \mathbf{F}_{i,l} = \left(\mathbf{T}^T \mathbf{K}_l \mathbf{T} + \mathbf{K}_{\sigma_1}\right)\delta\mathbf{u}_g = \mathbf{K}_T \delta\mathbf{u}_g \tag{29}$$

where $\mathbf{K}_{\sigma_1}$ is the initial stress matrix. This matrix can be determined using the variation of the transformation matrix $\mathbf{T}$

$$\delta\mathbf{T}^T \mathbf{F}_{i,l} = \delta\left[\left[\operatorname{diag}\,\mathbf{R}^T\right] + \operatorname{col}\left(\mathbf{R}^T \mathbf{S}\left(\mathbf{x}_g^{k_1}\right)\right)\mathbf{V}^T\right]\mathbf{F}_{i,l} = \mathbf{K}_{\sigma_1}\delta\mathbf{u}_g \tag{30}$$

If we define a local internal force vector $\widetilde{\mathbf{F}}_{i,l}^k$ for a node k such as,

$$\widetilde{\mathbf{F}}_{i,l}^k = \mathbf{R}\mathbf{F}_{i,l}^k \tag{31}$$

and then the initial stress matrix $\mathbf{K}_{\sigma_1}$ can take the form of

$$\mathbf{K}_{\sigma_1} = -\operatorname{col}\left(\mathbf{S}\left(\widetilde{\mathbf{F}}_{i,l}^k\right)\right)\mathbf{V}^T \; + \mathbf{V}\operatorname{row}\left(\mathbf{S}\left(\widetilde{\mathbf{F}}_{i,l}^k\right)\right) + \mathbf{V}\operatorname{row}\left(\mathbf{S}\left(\mathbf{x}_g^{k_1}\right)\right)\operatorname{col}\left(\mathbf{S}\left(\widetilde{\mathbf{F}}_{i,l}^k\right)\right)\mathbf{V}^T \tag{32}$$

however, last term in Eq.(32) produces non-symmetric matrix, we can write the non-symmetric part as

$$\mathrm{Non-sym} = \frac{1}{2}\sum_{k=1}^{n}\left(\mathbf{x}_g^{k_1}\widetilde{\mathbf{F}}_{i,l}^{kT} - \widetilde{\mathbf{F}}_{i,l}^k\mathbf{x}_g^{k1T}\right) \tag{33}$$

Then, the initial stress matrix $\mathbf{K}_{\sigma_1}$ is given by

$$\mathbf{K}_{\sigma_1} = -\operatorname{col}\left(\mathbf{S}\left(\widetilde{\mathbf{F}}_{i,l}^k\right)\right)\mathbf{V}^T \; + \mathbf{V}\operatorname{row}\left(\mathbf{S}\left(\widetilde{\mathbf{F}}_{i,l}^k\right)\right) + \mathbf{V}\operatorname{sym}\left(\sum_{k=1}^{n}\mathbf{S}\left(\mathbf{x}_g^{k_1}\right)\mathbf{S}\left(\widetilde{\mathbf{F}}_{i,l}^k\right)\right)\mathbf{V}^T \tag{34}$$

As a result, we can be write the stiffness matrices used in the incremental-iterative procedure in the matrix form as

$$\mathbf{K}^{uu} = \int \overline{\mathbf{B}}_l^{uT}\mathbf{D}\overline{\mathbf{B}}_l^u dV_0 \tag{35}$$

$$\mathbf{K}^{u\alpha} = \int \overline{\mathbf{B}}_l^{uT}\mathbf{D}\overline{\mathbf{B}}_l^\alpha dV_0 \tag{36}$$

$$\mathbf{K}^{\alpha\alpha} = \int \overline{\mathbf{B}}_l^{\alpha T} \mathbf{D} \overline{\mathbf{B}}_l^{\alpha} dV_0 \tag{37}$$

where $\mathbf{D}$ is the symmetric 6x6 material matrix.

And, the variable $\boldsymbol{\alpha}$ can be eliminated at the element level via

$$\delta\boldsymbol{\alpha} = (\mathbf{K}^{\alpha\alpha})^{-1} \left(\mathbf{K}^{u\alpha T} \delta\mathbf{u}_g - \mathbf{F}_{i,l}^{\alpha} \right) \tag{38}$$

$$\overline{\mathbf{F}}_{i,l} = \mathbf{F}_{i,l} - \mathbf{K}^{u\alpha} (\mathbf{K}^{\alpha\alpha})^{-1} \mathbf{F}_{i,l}^{\alpha} \tag{39}$$

$$\mathbf{K}_l = \mathbf{K}^{uu} - \mathbf{K}^{u\alpha} (\mathbf{K}^{\alpha\alpha})^{-1} \mathbf{K}^{u\alpha T} \tag{40}$$

$$\mathbf{K}_T = \mathbf{T}^T \mathbf{K}_l \mathbf{T} + \mathbf{K}_{\sigma_1} \tag{41}$$

where $\mathbf{K}_T$ is the tangent stiffness matrix. And, we can determine the out of balance force $\mathbf{P}$ used in the nonlinear procedure as

$$\mathbf{P} = \mathbf{F}_e - \mathbf{T}^T \overline{\mathbf{F}}_{i,l} \tag{42}$$

where $\mathbf{F}_e$ is the external force.

2.5   The solution method

In order to compute the nodal displacements, the load controlled Newton-Raphson method and the spherical arc-length algorithm with the predictor criterion of Refs. [6, 7] are used. The convergence criteria is chosen as

$$\|\delta\mathbf{u}_g\| < 10^{-5} \|\Delta\mathbf{u}_g\| \tag{43}$$

where δ and Δ parameters indicate iterative and incremental quantities, respectively.

3   NUMERICAL EXAMPLES

The element stiffness matrix is computed numerically using a 2×2×2 Gauss integration scheme. Most of the results presented here are compared with solutions of Sze. et al. [8] who chosen S4R element in their analysis.

3.1   A cantilever subjected to end shear force

A cantilever is subjected to an end shear force F, shown in Figure 2. The problem is examined using 20x1x1 enhanced brick elements. Figure 3 plots the end shear force against the vertical and horizontal tip displacements of both present and 16x1 S4R element results. The difference between two analyses is almost indistinguishable.

$E = 1.2 \times 10^6$

$\nu = 0$

$L = 10$

$b = 1$

$h = 0.1$

$F = 4$
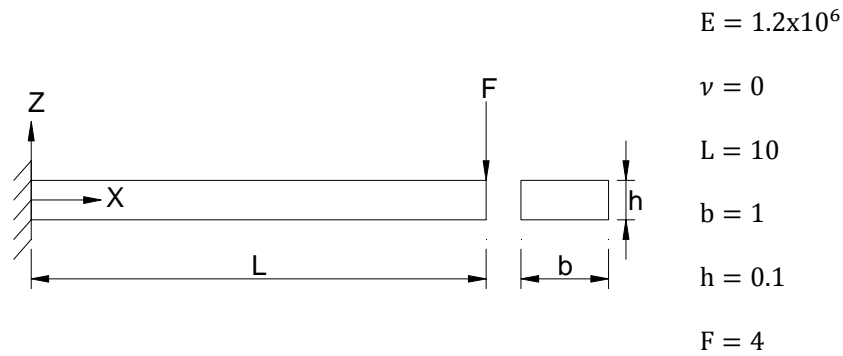
Figure 2   Cantilever subjected to end shear force.
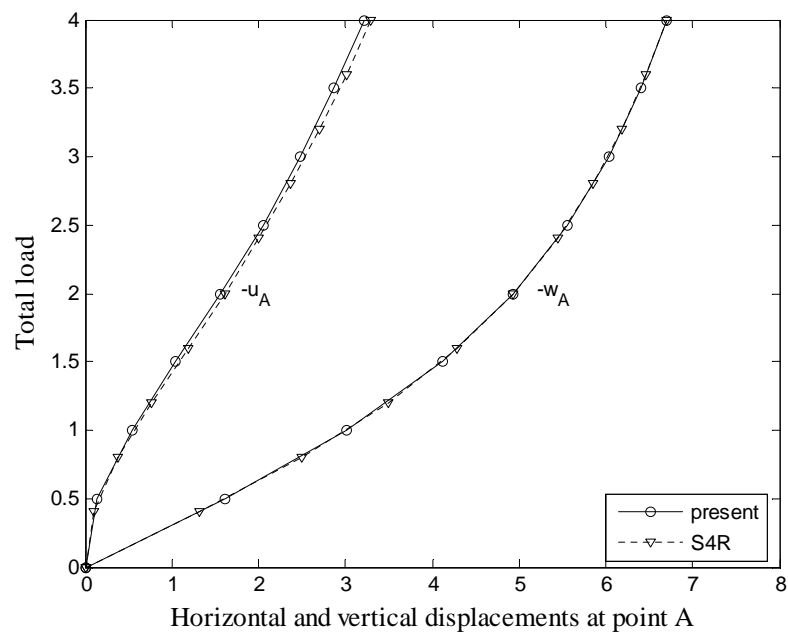
Figure 3   Load-displacement curves for cantilever subjected to end shear force.

3.2   A 45° circular cantilever with large displacements and large rotations

A 45° bend cantilever is provided with a concentrated end load in Z-direction. The bend has a radius of 100 and a square cross-section of 1x1, as illustrated in Figure 4. The cantilever is meshed using 20x2x2 enhanced brick elements. Four load increments are employed to calculate the tip displacements under the given load level. Figure 5 presents the tip displacements for different load steps.
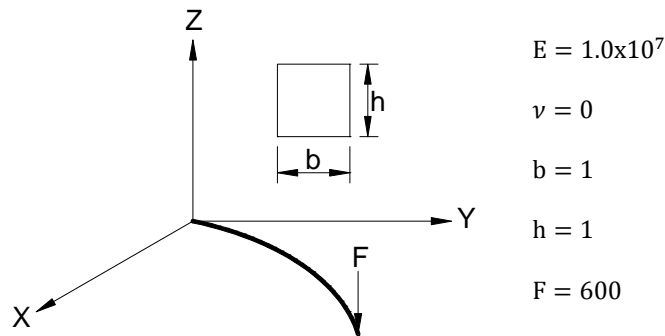
Figure 4   A cantilever 45° bend with a concentrated tip load.

$E = 1.0 \times 10^7$

$\nu = 0$

$b = 1$

$h = 1$

$F = 600$
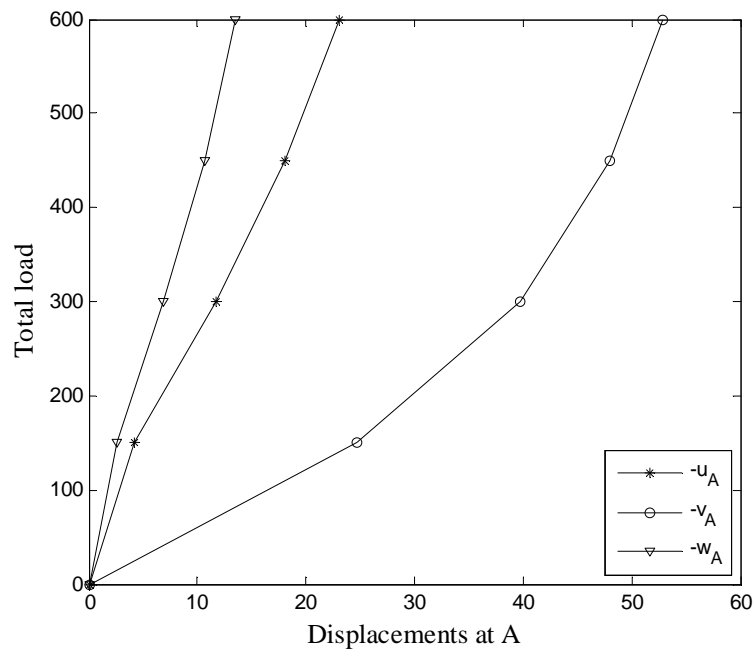
Figure 5   Load-displacement curves for the bend cantilever.

3.3   Slit annular plate under line force

A circular annular plate with inner radius R_i and outer radius R_o is shown in Figure 6. It has a radial rip and is modeled by 8x48x1enhanced brick elements. A line force is applied at its free edge while the other edge is fully clamped. The maximum line force is 0.8 units of force per unit length. Vertical displacements obtained for points A and B are plotted versus the load on the Figure 7. As it can be seen, the results presented herein converge properly to the 10x80 S4R element results.

$E = 2.1x10^7$

$\nu = 0$

$R_i = 6$

$R_o = 10$

$h = 0.03$
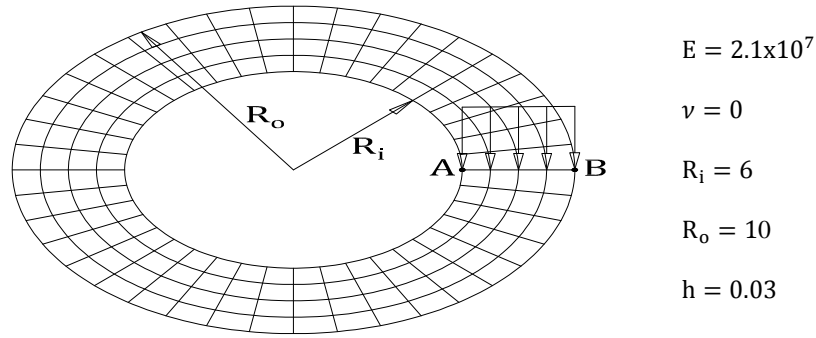
Figure 6   The slit annular plate loaded with the line force.
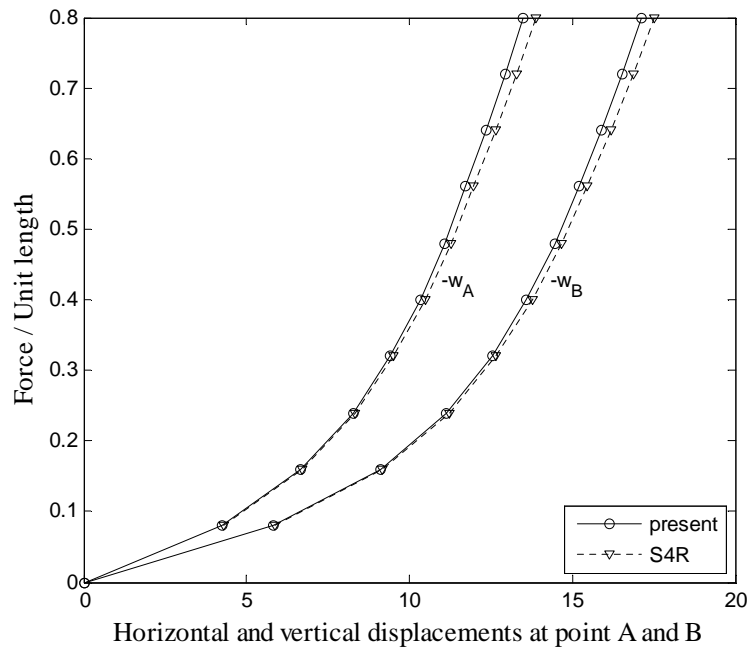
Figure 7   Load-displacement curves for the slit annular plate.

3.4   Hinged semi-cylindrical roof

This is a commonly used test case for large-displacement analysis of shallow shell subjected to a central pinching force, see Figure 8. The straight edges are hinged and immovable while the curved edges are free. The structure is modeled with 10x10x2 enhanced brick elements on one quarter of its surface and along with two elements over the thickness direction. We investigate the buckling behavior of the cylindrical shell for two different thicknesses. The vertical displacements of points A are reproduced in Figure 9 and 10, plotted against the load level and compared to the S4R element solutions. A very good agreement between the solutions along the entire unstable load-displacement path is noticeable.
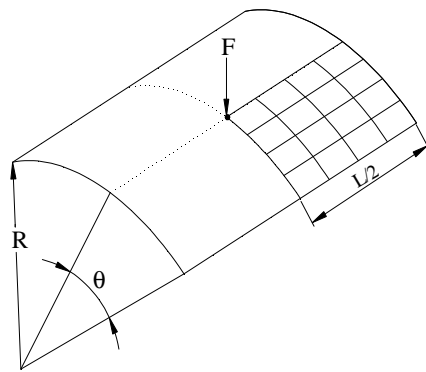
$E = 3102.75$

$\nu = 0.3$

$R = 2540$

$L = 508$

$\theta = 0.1 \text{ rad}$

$h = 12.7$

or

$h = 6.35$

Figure 8   Hinged semi-cylindrical roof subjected to a central point load.
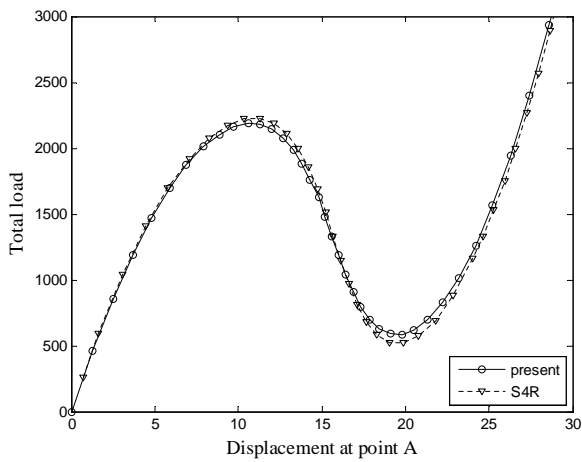
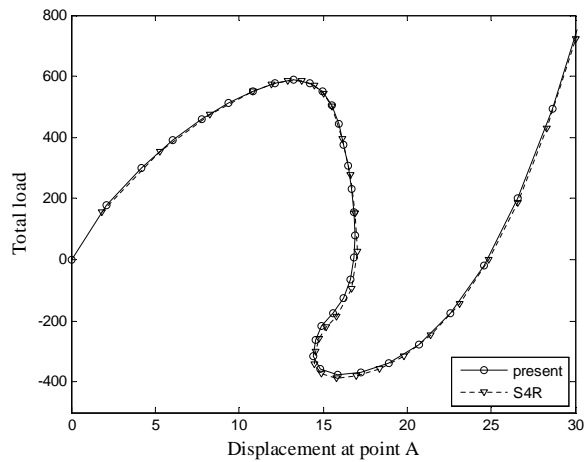Figure 9   Load-displacement curves for the hinged semi-cylindrical roof for $h = 12.7$.

Figure 10   Load-displacement curves for the hinged semi-cylindrical roof for $h = 6.35$.

3.5   Pull-out of an open cylinder

A cylinder is pinched by two radially pulling forces F as shown in Figure 11. Both ends of the cylinder are free. One quarter of the cylinder is discretized and the corresponding symmetry is taken into account. The structure is modeled with 24x36x1 enhanced brick elements. The results are shown in Figure 12 which presents radial displacement of points A, B and C with respect to the magnitude of the applied forces. There is a slight snap-through behavior of the solution when load equals to approximately 20680.
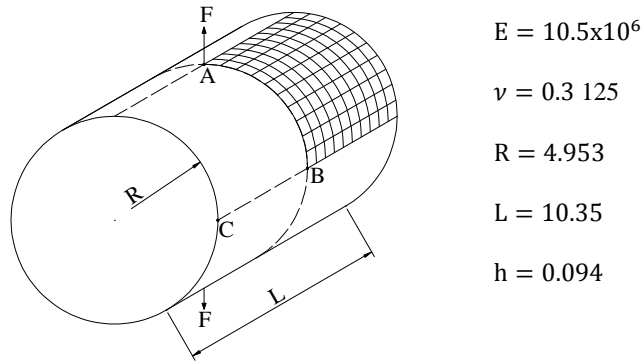
$$E = 10.5 \times 10^6$$

$$\nu = 0.3\ 125$$

$$R = 4.953$$

$$L = 10.35$$

$$h = 0.094$$
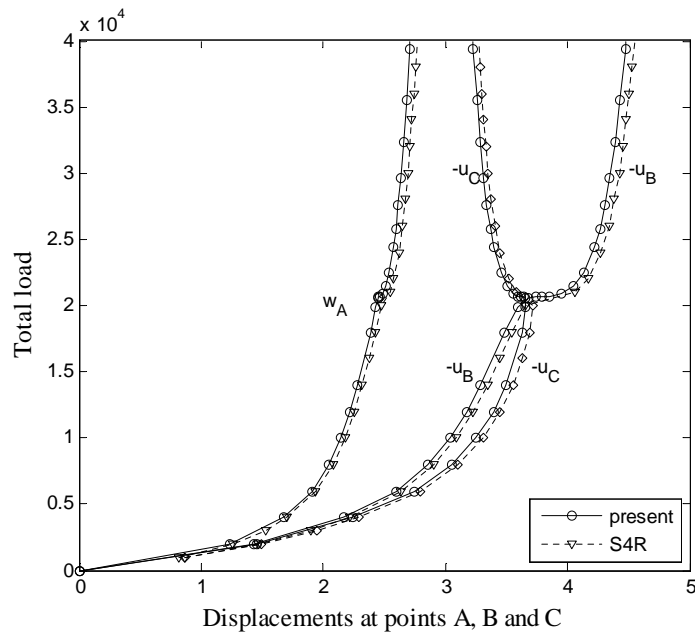
Figure 11   Pull-out of an open cylinder.

Figure 12   Load-displacement curves for the open cylinder.

4   CONCLUSIONS

A locking free formulation of 8-node brick element based on the co-rotational description of motion was demonstrated. The EAS method was used to circumvent the locking phenomenon of the element. The polar decomposition theorem was employed to obtain the rotation matrix and the transformation matrix which defines the relationship between the variation of the local displacements and the variation of the global displacements was also formed. Thus, geometric nonlinearities were taken into account via rotation of the local system. Analyzed benchmark problems showed that the proposed method is reliable and effective. Moreover, it is easy to perform.

References

[1] U. Andelfinger and E. Ramm. Eas-elements for two-dimensional, three-dimensional, plate and shell structures and their equivalence to HR-elements. *International Journal for Numerical Methods in Engineering*, 36:1311–1337, 1993.

[2] J.H. Argyris, H. Balmer, J. Doltsnis, et al. Finite element method-the natural approach. *Computer Methods in Applied Mechanics and Engineering*, 17/18:l–106, 1979.

[3] T. Belytschko and L.W. Glaum. Application of higher order corotational stretch theories to nonlinear finite element analysis. *Computers and Structures*, 10:175–182, 1979.

[4] M.A. Crisfield and G.F. Moita. A co-rotational formulation for 2-D continua including incompatible modes. *International Journal of Numerical Methods in Engineering*, 39:2619–2633, 1996.

[5] C.A. Felippa and B. Haugen. A unified formulation of small strain corotational finite elements: I. Theory. *Computer Methods in Applied Mechanics and Engineering*, 194:2285–2335, 2005.

[6] Y.T. Feng, D. Peric, and D.R.J. Owen. Determination of travel directions in path-following methods. *Mathematical and Computer Modelling*, 21:43–59, 1995.

[7] Y.T. Feng, D. Peric, and D.R.J. Owen. A new criterion for determination of initial loading parameter in arc-length methods. *Computers & Structures*, 58:479–485, 1996.

[8] Sze K.Y., X.H. Liu, and S.H. Lo. Popular benchmark problems for geometric nonlinear analysis of shells. *Finite Elements in Analysis and Design*, 40:1551–1569, 2004.

[9] G.F. Moita and M.A. Crisfield. A finite element formulation for 3-d continua using the co-rotational technique. *International Journal of Numerical Methods in Engineering*, 39:3775–3792, 1996.

[10] Klinkel S. and Wagner W. A geometrical non-linear brick element. *International Journal for Numerical Methods in Engineering*, 40:4529–4545, 1997.

[11] J.C. Simo and M.S. Rifai. A class of mixed assumed strain methods and the method of incompatible modes. *International Journal for Numerical Methods in Engineering*, 29:1595–1638, 1990.

[12] R.J.A. Sousa, R.P.R. Cardoso, R.A.F. Valente, J.W. Yoon, J.J. Gracio, and R.M.N. Jorge. A new one-point quadrature enhanced assumed strain solid-shell element with multiple integration points along thickness. Part II – Nonlinear Applications. *International Journal of Numerical Methods in Engineering*, 67:160–188, 2006.

[13] Y. Urthaler and J.N. Reddy. A corotational finite element formulation for the analysis of planar beams. *Communications in Numerical Methods in Engineering*, 21:553–570, 2005.

[14] R.A.F. Valente. *Developments on shell and solid-shell finite elements technology in nonlinear continuum mechanics.* PhD thesis, University of Porto, Portugal, 2004.

[15] G. Wempner. Finite elements, finite rotations and small strains of flexible shells. *The International Journal of Solids and Structures*, 5:117–153, 1969.